



## Pulse reverse engineering for controlling two-level quantum systems

Du Ran <sup>1,2,3</sup> Wu-Jiang Shan,<sup>4</sup> Zhi-Cheng Shi,<sup>1,\*</sup> Zhen-Biao Yang,<sup>1</sup> Jie Song <sup>5</sup> and Yan Xia<sup>1,†</sup>

<sup>1</sup>*Fujian Key Laboratory of Quantum Information and Quantum Optics (Fuzhou University), Fuzhou 350116, China*

<sup>2</sup>*School of Electronic Information Engineering, Yangtze Normal University, Chongqing 408100, China*

<sup>3</sup>*Department of Electrical Engineering Physical Electronics, Tel Aviv University, Ramat Aviv 69978, Israel*

<sup>4</sup>*School of General Education, Jiangxi Vocational College of Industry and Engineering, Pingxiang 337055, China*

<sup>5</sup>*Department of Physics, Harbin Institute of Technology, Harbin 150001, China*



(Received 1 September 2019; revised manuscript received 15 December 2019; accepted 21 January 2020; published 14 February 2020)

In this paper, based on the idea of reverse engineering, we propose a scheme to find analytical expressions of a laser pulse that allows for controlling the evolution of two-level systems as desired, regardless of the time-dependent phase of the system. The pulse relates to particular functions that predefine the evolution of a system. For illustration, we present concrete examples of driving the system from an arbitrary initial state to a final state along the user-prescribed particular way in both closed and open quantum systems. Simulation results indicate that the desired evolutionary path is accurately obtained when the rotating wave approximation (RWA) is satisfied. Most importantly, the scheme allows us to maintain system coherence and populations even in the presence of certain dephasing and thermal noises. Thus it may naturally find applications in quantum computing and quantum memories.

DOI: [10.1103/PhysRevA.101.023822](https://doi.org/10.1103/PhysRevA.101.023822)

### I. INTRODUCTION

The control of quantum systems has long been the central interest of quantum science [1–10]. For example, transferring population between individual discrete quantum states of atoms and molecules is fundamental in modern atomic and molecular physics [11,12]. The methods for population transition include adiabatic control [13–15], shortcut-to-adiabaticity (STA) [16–18], optimal control [19–21], Lyapunov control [22–28], measurement-feedback control [29–31], and so on. Among these impressive achievements, adiabatic control technique has been holding an irreplaceable position in the field of population transition due to its robustness against small-to-moderate variations in control parameters [32]. However, the extension of adiabatic passage to the open quantum systems may be a difficult task since adiabatic processes generally require relatively long times so that decoherence would seriously decline system dynamics [33]. In the context of a dissipative system, several studies using numerical and analytical techniques proved that efficient control can still be achieved [34–37]. To relax the restrictions of adiabatic condition required in adiabatic control, STA accelerates adiabatic processes by designing pulses [38,39]. Other pulse-design methods such as optimal control and Lyapunov control are also appreciated [40–42] since the crafted external electromagnetic radiation fields are always necessary for implementing varieties of quantum control tasks [43–47], including population transition.

For population transition, the traditional pulse-design methods are typically used to drive the interested system into

a desired final state, sometimes along one specific instantaneous eigenstate [48,49], instead of controlling the evolution path of system arbitrarily. For instance, by suppressing nonadiabatic transitions, STA transports an initial state to a final state along a chosen state trajectory which is an instantaneous eigenstate of original Hamiltonian [50,51]. By combining STA with optimal control, robust population transition along specific trajectory is realized in a  $\Lambda$  system [52]. Fast adiabatic evolution is achieved by constructing effective counterdiabatic Hamiltonian [53]. Daems *et al.* [54] established a strategy based on an inverse-engineering protocol that allows a robust and precise transfer to a given target state.

To achieve arbitrary user-prescribed evolution path, Golubev *et al.* [55] proposed a scheme based on the idea of reverse engineering to obtain laser pulse for controlling populations of two-level systems, which allows one to drive the system from any initial state into a desired final state. Later, they applied the approach for finding laser pulse to control the charge migration in a real molecule [56]. However, the pulse may hardly be obtained when the phase of amplitude of eigenstate  $|g(e)\rangle$  is time-dependent, i.e., the phases  $\phi_j$  ( $j = 1, 2$ ) of the complex amplitudes  $c_j(t) = \tilde{c}_j(t)e^{i\phi_j}$  are time-varying, where  $c_j(t)$  satisfy  $\sum_{j=1}^2 |c_j(t)|^2 = 1$ ,  $|\psi(t)\rangle = c_1(t)|g\rangle + c_2(t)|e\rangle$ , and  $\tilde{c}_j(t)$  are real positive. In addition, the reverse-engineering approach is merely applicable for the closed quantum systems, originating from the fact that the pulse is obtained based on the wave function of the system. Recently, the reverse-engineering idea achieved significant progress, which is generalized to the more realistic scenarios to include dephasing and thermal noises based on the density matrix of a system instead of the wave function [57]. Noticeably, the pulse is also quite difficult to obtain when the

\*szc2014@yeah.net

†xia-208@163.com

phase of coherence is time-dependent, i.e., the phase  $\phi'$  in  $\rho_{ge} = |\rho_{ge}|e^{i\phi'}$  is time-varying.

Inspired by previous works [55–57], in this paper, we propose an alternative scheme to obtain analytical expressions of laser pulse for controlling the evolution path of two-level systems as desired. First, we predefine the evolution of the system by the user-prescribed population control function (PCF) and coherence control function (CCF). By reversely solving the master equation of motion, we then obtain the laser pulse that relates to the predefined PCF and CCF. Thus, the reverse-engineering scheme sidesteps the consideration of the phase of amplitude and the phase of coherence during designing the laser pulse. The dominant feature of the scheme is that it is suitable for both closed and open quantum systems, enabling for controlling not only the final-state superposition but also the exact evolution path. In addition, each final state is achievable for closed quantum systems, while for open quantum systems, there are unaccessible final states and we shall discuss the limitations for that. We believe that the scheme is a valuable addition to the arsenal of quantum control, especially involving qubits driven by external fields in a noisy environment.

The rest of this paper is organized as follows. In Sec. II, we present the system model and the idea of pulse reverse engineering. In Sec. III, we present some illustration examples in the closed and open quantum systems. In Sec. IV, we discuss the robustness of the scheme and the accessible regions for the population transition in the open quantum system case. Conclusions are presented in Sec. V.

## II. SYSTEM MODEL AND PULSE REVERSE ENGINEERING

Let us consider the most common model: a two-level system interacts with a classical monochromatic field. The two-level system has a ground state  $|g\rangle$  and an excited state  $|e\rangle$  with eigenenergies  $\hbar\omega_g$  and  $\hbar\omega_e$ , respectively. The interaction between the states  $|g\rangle$  and  $|e\rangle$  is of electric dipole form. For instance, for an atom interacting with a laser pulse, such electric dipole approximation is valid when the wavelengths of the pulse are much greater than the mean spatial separation of the electron and the nucleus [58]. The Hamiltonian in this dipole approximation case has the following form (we set  $\hbar = 1$  hereafter)

$$\hat{H}(t) = -\frac{\omega}{2}\hat{\sigma}_z - \boldsymbol{\mu} \cdot \mathbf{E}(t)\hat{\sigma}_x, \quad (1)$$

where  $\omega = \omega_e - \omega_g$  is the two-level system transition frequency, and  $\hat{\sigma}_j$  ( $j = x, y, z$ ) are the pseudospin operators, namely Pauli operators. For regular use later, we further introduce the raising or lowering operators:  $\hat{\sigma}_{\pm} = (\hat{\sigma}_x \pm i\hat{\sigma}_y)/2$ . The electric dipole operator  $\boldsymbol{\mu}$  is given by  $\boldsymbol{\mu} = \mathbf{e}_{\mu}(\mu|g\rangle\langle e| + \mu^*|e\rangle\langle g|)$  with  $\mathbf{e}_{\mu}$  being the unit vector in the direction of the dipole and  $\mu$  denoting the matrix element of the dipole operator between states  $|g\rangle$  and  $|e\rangle$ . The pulse  $\mathbf{E}(t)$  with carrier frequency  $\omega_p$  can be written as

$$\mathbf{E}(t) = \boldsymbol{\varepsilon}(t)e^{-i\omega_p t} + \boldsymbol{\varepsilon}^*(t)e^{i\omega_p t}, \quad (2)$$

where  $\boldsymbol{\varepsilon}(t)$  contains the polarization, amplitude, and envelope of the pulse  $\mathbf{E}(t)$ . For simplicity, we assume  $\mu$  is real and take the scalar product between  $\boldsymbol{\mu}$  and  $\mathbf{E}(t)$ , i.e.,  $\boldsymbol{\mu} \cdot \mathbf{E}(t) = \mu E(t)$ .

For convenience, we move to the interaction picture with respect to  $\hat{U}(t) = \exp[i\frac{\omega}{2}\hat{\sigma}_z t]$ . Then the Hamiltonian  $H(t)$  under the RWA reads

$$\hat{H}_I(t) = -\mu[\varepsilon(t)\hat{\sigma}_+ e^{-i\Delta t} + \varepsilon^*(t)\hat{\sigma}_- e^{i\Delta t}], \quad (3)$$

where the detuning  $\Delta = \omega_p - \omega$ . We take into account the presence of dephasing and thermal noises caused by environment with rates  $\gamma$  and  $\Gamma$ , respectively. Then, the general form of the density matrix describing the evolution of the system is given by the following equation [59]:

$$\dot{\hat{\rho}}(t) = -i[\hat{H}_I(t), \hat{\rho}(t)] + \frac{\gamma}{2}D_{de}[\hat{\rho}(t)] + \Gamma D_{th}[\hat{\rho}(t)], \quad (4)$$

where  $D_{de}[\hat{\rho}(t)] = \hat{\sigma}_z \rho(t) \hat{\sigma}_z - \hat{\rho}(t)$  and  $D_{th}[\hat{\rho}(t)] = \bar{n}[2\hat{\sigma}_+ \hat{\rho}(t) \hat{\sigma}_- - \{\hat{\sigma}_- \hat{\sigma}_+, \hat{\rho}(t)\}] + (\bar{n} + 1)[2\hat{\sigma}_- \rho(t) \hat{\sigma}_+ - \{\hat{\sigma}_+ \hat{\sigma}_-, \hat{\rho}(t)\}]$  with  $\bar{n}$  being the effective photon number. This equation can be solved by directly solving the elements of the density matrix [57]. Here we represent the density matrix in the following form, which defines arbitrary evolution of two-level system [60],

$$\begin{aligned} \hat{\rho}(t) &= \frac{1}{2}[\hat{\mathbb{I}} + u(t)\hat{\sigma}_x + v(t)\hat{\sigma}_y + w(t)\hat{\sigma}_z] \\ &= \frac{1}{2} \begin{bmatrix} 1 + w(t) & u(t) - iv(t) \\ u(t) + iv(t) & 1 - w(t) \end{bmatrix}, \end{aligned} \quad (5)$$

where  $\hat{\mathbb{I}}$  is the identity operator, and the real functions  $u(t)$ ,  $v(t)$ ,  $w(t)$  are

$$\begin{aligned} u(t) &= \text{Tr}[\hat{\sigma}_x \hat{\rho}(t)] = \rho_{eg} + \rho_{ge}, \\ v(t) &= \text{Tr}[\hat{\sigma}_y \hat{\rho}(t)] = i(\rho_{eg} - \rho_{ge}), \\ w(t) &= \text{Tr}[\hat{\sigma}_z \hat{\rho}(t)] = \rho_{ee} - \rho_{gg}, \end{aligned} \quad (6)$$

with  $\rho_{nm}$  ( $m, n = g, e$ ) denoting the matrix elements of  $\hat{\rho}(t)$ . Then, it is not hard to calculate from Eqs. (4) and (5) that

$$\dot{u} = -\tilde{\Gamma}u - i\mu w(\varepsilon e^{-i\Delta t} - \varepsilon^* e^{i\Delta t}), \quad (7a)$$

$$\dot{v} = -\tilde{\Gamma}v + \mu w(\varepsilon e^{-i\Delta t} + \varepsilon^* e^{i\Delta t}), \quad (7b)$$

$$\dot{w} = -\frac{[u(\dot{u} + \tilde{\Gamma}u) + v(\dot{v} + \tilde{\Gamma}v)]}{w} - 4\bar{n}\Gamma w - 2\Gamma(w + 1), \quad (7c)$$

where  $\tilde{\Gamma} = [(2\bar{n} + 1)\Gamma + \gamma]$  is the total decoherence rate. Note that we ignored “(t)” for the sake of brevity.

The goal here is to find the pulse  $E(t)$  which will drive the system to evolve as user-prescribed. Notice that  $\varepsilon(t)e^{-i\Delta t} = \varepsilon(t)e^{-i\omega_p t} e^{i\omega t} \equiv a + ib$ , where we define  $a = \text{Re}[\varepsilon(t)e^{-i\Delta t}]$  and  $b = \text{Im}[\varepsilon(t)e^{-i\Delta t}]$  ( $\text{Re}[\cdot]$  and  $\text{Im}[\cdot]$  represent the real and imaginary parts of the argument, respectively). To achieve the goal, we reversely solve Eq. (7) and obtain

$$a = \frac{1}{2\mu w}(\dot{v} + \tilde{\Gamma}v), \quad (8a)$$

$$b = \frac{1}{2\mu w}(\dot{u} + \tilde{\Gamma}u), \quad (8b)$$

$$u\dot{u} + v\dot{v} + w\dot{w} = -2\Gamma(2\bar{n} + 1)w^2 - 2\Gamma w - \tilde{\Gamma}(u^2 + v^2). \quad (8c)$$

Then the pulse  $E(t)$  in the presence of dephasing and thermal noises reads

$$E(t) = \frac{1}{\mu w} [(\dot{v} + \tilde{\Gamma}v) \cos(\omega t) + (\dot{u} + \tilde{\Gamma}u) \sin(\omega t)]. \quad (9)$$

It is worth mentioning that the functions  $u(t)$ ,  $v(t)$ , and  $w(t)$  are bounded by Eq. (8c). Thus when giving two concrete expression among the functions  $u(t)$ ,  $v(t)$ , and  $w(t)$ , the remaining one is achieved from Eq. (8c). For instance, given the functions  $v(t)$  and  $w(t)$ , the  $u(t)$  reads

$$u(t) = \pm \sqrt{y(t)},$$

$$y(t) = 2e^{-2\tilde{\Gamma}t} \int_0^t e^{2\tilde{\Gamma}\tau} f(\tau) d\tau + y(-\infty)e^{-2\tilde{\Gamma}t}, \quad (10)$$

where  $f(t) = -w\dot{w} - v\dot{v} - \tilde{\Gamma}v^2 - 4\tilde{n}\Gamma w^2 - 2\Gamma w(w+1)$ . Similarly, one can also give the concrete forms of  $u(t)$  and  $w(t)$ , then obtain the function  $v(t)$  as  $v(t) = \pm \sqrt{y'(t)}$  with  $y'(t) = 2e^{-2\tilde{\Gamma}t} \int_0^t e^{2\tilde{\Gamma}\tau} f'(\tau) d\tau + y'(-\infty)e^{-2\tilde{\Gamma}t}$ , where  $f'(t) = -w\dot{w} - u\dot{u} - \tilde{\Gamma}u^2 - 4\tilde{n}\Gamma w^2 - 2\Gamma w(w+1)$ . However, if we predefine the functions  $u(t)$  and  $v(t)$ , the analytic expression of  $w(t)$  is unobtainable. In this case, one can obtain the values of  $w(t)$  by numerical calculations in principle.

Until now, we demonstrate the connection between the evolution of system and the pulse  $E(t)$ . That is, by giving two of the functions  $u(t)$ ,  $v(t)$ , and  $w(t)$ , the pulse  $E(t)$  is determined by Eq. (9), which will guide the evolution of system as user-prescribed. Since  $w(t)$  confines the evolution of the population, we refer to the function  $w(t)$  as the population control function (PCF). From Eq. (5), we note that the functions  $u(t)$  and  $v(t)$  define the evolution of the coherence due to  $\rho_{ge} = \frac{1}{2}[u(t) - iv(t)]$ . Thus, we refer to the function  $C_A(t) = \frac{1}{2}|u(t) - iv(t)|$  as the coherence control function (CCF). It is clear that the present reverse-engineering method is universal over previous schemes [55–57] because the density matrix formula Eq. (5) is, in fact, applicable to any two-level systems. To be concrete, for closed quantum systems, we can represent the wave function  $|\psi(t)\rangle = c_1(t)|g\rangle + c_2(t)|e\rangle$  of the system in the density matrix formula as

$$\hat{\rho} = |\psi(t)\rangle\langle\psi(t)| = \begin{bmatrix} \tilde{c}_1^2(t) & \tilde{c}_1(t)\tilde{c}_2(t)e^{i\phi} \\ \tilde{c}_1(t)\tilde{c}_2(t)e^{-i\phi} & \tilde{c}_2^2(t) \end{bmatrix}, \quad (11)$$

where  $c_j(t) = \tilde{c}_j(t)e^{i\phi_j}$  ( $j = 1, 2$ ),  $|c_1(t)|^2 + |c_2(t)|^2 = 1$ , and  $\phi = \phi_1 - \phi_2$  is the relative phase between the amplitudes  $c_1(t)$  and  $c_2(t)$ . The pulse proposed by the authors of Ref. [55] only relates to the population control function  $c_1^2(t)$ , and requires that the phases  $\phi_1$  and  $\phi_2$  are time-independent. However, the pulse given by Eq. (9) relates to not only the PCF but also the CCF. The increased flexibility in designing the pulse provides us one more degree of freedom for controlling the system, i.e., the real component  $u(t)$  [or the imaginary component  $v(t)$ ] of coherence. It also avoids the consideration of the phases  $\phi_j$  ( $j = 1, 2$ ) of amplitudes. In addition, the pulse may hardly be obtained by reversely solving the optical Bloch equations for population control under dephasing and dissipation [57] when the phase  $\phi'$  of  $\rho_{ge} = |\rho_{ge}|e^{i\phi'}$  is time-dependent, which is also sidestepped in the present reverse-engineering method. In addition, the coherence of system is

solvable only in the case of long time evolution (the case of steady states) in Ref. [57]. It is clear that another advantage of the current reverse-engineering method over the previous one [57] is that not only the path of population transition but also the coherence of system are predictable at each moment.

### III. ILLUSTRATION EXAMPLES

For facilitating a comparison to the existing techniques [55–57], let us illustrate the present reverse-engineering method by some concrete examples. Suppose that the function  $w(t)$  has the following form:

$$w(t) = a_i[1 - g(t)] + a_f g(t), \quad (12)$$

where  $g(t) = 1/[1 + \exp(-\alpha t)]$  goes smoothly from 0 to 1 with a real and positive parameter  $\alpha$  controlling the duration of transition  $a_i \rightarrow a_f$  ( $a_i, a_f \in [-1, 1]$ ). According to Eq. (5), one notes that the function  $w(t)$  relates to the evolution of population  $P_{g(e)} = \langle g(e)|\hat{\rho}(t)|g(e)\rangle$ . Concretely, since  $g(t)$  goes smoothly from 0 to 1, resulting in  $w(t)$  varying in range  $[a_i, a_f]$ , so that  $a_i \xrightarrow{w(t)} a_f$  corresponds to  $\frac{1+a_i}{2} \xrightarrow{P_g} \frac{1+a_f}{2}$  and  $\frac{1-a_i}{2} \xrightarrow{P_g} \frac{1-a_f}{2}$ . The function  $v(t)$  can be arbitrarily chosen in principle. Here, it is considered to be the Gaussian form  $v(t) = Ae^{-\frac{1}{2}(t-\tau)^2/\sigma^2}$ , where the real parameter  $A \in [0, 1]$  is the height of the curve's peak,  $\tau$  is the position of the center of the peak, and  $\sigma$  controls the width of the “bell.” Therefore, after giving the specific PCF  $w(t)$  and CCF  $C_A(t)$ , one can fully control the evolution of the system as desired with the control field given by Eq. (9).

#### A. Illustration I: Closed Quantum System

For the purpose of illustration, we first consider the case of absence of dephasing and thermal noises, i.e.,  $\Gamma = \gamma = 0$  a.u., where atomic units are used throughout the paper unless otherwise specified. We substitute the pulse  $E(t)$  [given by Eq. (9)] into the Hamiltonian  $H(t)$  in Eq. (1), and numerically solve the equation of motion for the system without RWA, i.e.,  $\dot{\hat{\rho}}(t) = -i[\hat{H}(t), \hat{\rho}(t)]$ . The simulation results are presented in Fig. 1, together with the prescribed functions and pulse  $E(t)$ . In the simulation, we choose the parameters  $a_i = 1$  and  $a_f = -1$ , where  $a_i = 1$  and  $a_f = -1$  correspond to  $w(-\infty) = 1$  [ $\hat{\rho}(-\infty) = |e\rangle\langle e|$ ] and  $w(+\infty) = -1$  [ $\hat{\rho}(+\infty) = |g\rangle\langle g|$ ], respectively. It is also worth mentioning that the value of  $a_{i(f)}$  can be arbitrarily chosen in the range  $[-1, 1]$ , which provides us the freedom to choose the desired final state starting from arbitrary initial one.

Figure 1(a) depicts the PCF  $w(t)$  and the evolution of  $\langle \hat{\sigma}_z \rangle = \text{Tr}[\hat{\sigma}_z \hat{\rho}(t)]$ , where  $\hat{\rho}(t)$  is numerically solved without RWA. It is clear that the evolution of  $\langle \hat{\sigma}_z \rangle$  (red dash line) closely follows the PCF  $w(t)$  (blue solid line) with small deviations. Figure 1(b) shows the CCF  $C_A(t)$  and the evolution of coherence defined as  $C_N(t) = |\langle g|\hat{\rho}(t)|e\rangle|$  [57]. We note that  $C_N(t)$  coincides with  $C_A(t)$  very well when  $t < 0$  a.u., while there occurs small variations from then on, and finally  $C_N(t)$  plateaus to a finite value as  $C_N(+\infty) \rightarrow 0.1$ . The population evolutions of  $P_g = \langle g|\hat{\rho}(t)|g\rangle$  and  $P_e = \langle e|\hat{\rho}(t)|e\rangle$  are shown in Fig. 1(c), from which one observes the perfect population inverting, where  $P_g$  reaches 0.996 when the evolution time is

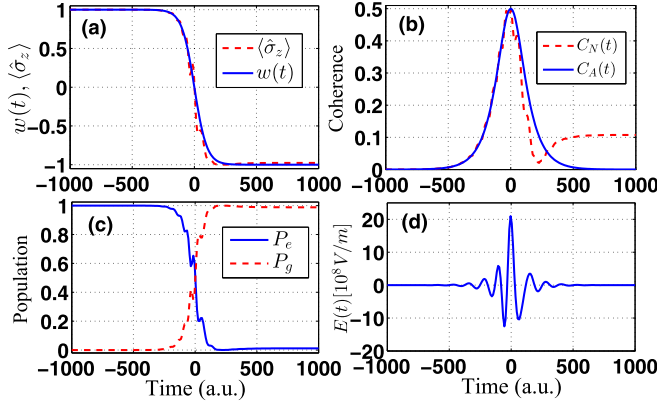


FIG. 1. (a) The PCF  $w(t)$  and the  $\langle \hat{\sigma}_z \rangle$  as a function of time. (b) The analytical  $[C_A(t)]$  and numerical  $[C_N(t)]$  coherence as a function of time. (c) The evolution of ground-state population  $P_g$  and excited state population  $P_e$ . (d) The field obtained from Eq. (9) with the following parameters:  $a_i = 1$ ,  $a_f = -1$ ,  $\alpha = 0.02$  a.u.,  $\omega = 0.05$  a.u.,  $A = 0.6$  a.u.,  $\tau = 0$  a.u.,  $\sigma = 50$  a.u.,  $\Gamma = \gamma = 0$  a.u., and  $\mu = 6$  a.u.

226.1 a.u. Figure 1(d) shows the pulse  $E(t)$  obtained from Eq. (9). From the simulation, one notes that the evolution of population performs very well, while the evolution of coherence slightly deviates from the desired one. The reason for being unable to fully control the evolution of the system arises from the fact that the RWA is not strictly satisfied for the chosen parameters. It is known that the RWA usually works well only if the system is nearly resonant driven [55]. Thus, whether the RWA well is satisfied or not influences the degree of precision in controlling the evolution of system. This point will be discussed in the next section.

As we mentioned previously, the pulse  $E(t)$  is related to the predefined evolution of the two-level system determined by the functions  $u(t)$ ,  $v(t)$ , and  $w(t)$ . That is, there is a consistent one-to-one match between a given trajectory on the Bloch sphere and the pulse. For each given trajectory, the corresponding pulse area is a parameter of importance for the control. Here we investigate the pulse area  $A_{\text{pulse}} = \mu \int E(t) dt$  for different trajectories and compare it with the  $\pi$  pulse. Figure 2 depicts five different trajectories on the Bloch sphere, in which the trajectory of  $\pi$  pulse is generated with the Hamiltonian  $H_\pi = \frac{\Omega}{2}[\sigma_+ \exp(i\theta) + \sigma_- \exp(-i\theta)]$ . We can see from Fig. 2 that the trajectories (with different  $\alpha$ ) approach the  $\pi$ -pulse trajectory when increasing the value of  $\alpha$ . However, the pulse area decreases with the increasing the value of  $\alpha$ . This originates from the fact that  $\alpha$  controls the speed of the dynamics, the bigger the  $\alpha$  the shorter the pulse.

## B. Illustration II: Open Quantum System

As we mentioned above, one feature of the scheme is that it allows us to control the evolution of quantum systems as desired. Generally, the populations and the coherence of system will be unavoidably influenced by the environment. In the following, we study the reverse-engineering scheme in the open quantum system by taking into account the presence of dephasing and thermal noises. First, we consider the influence of pure dephasing by setting  $\Gamma = \bar{n} = 0$  a.u. One

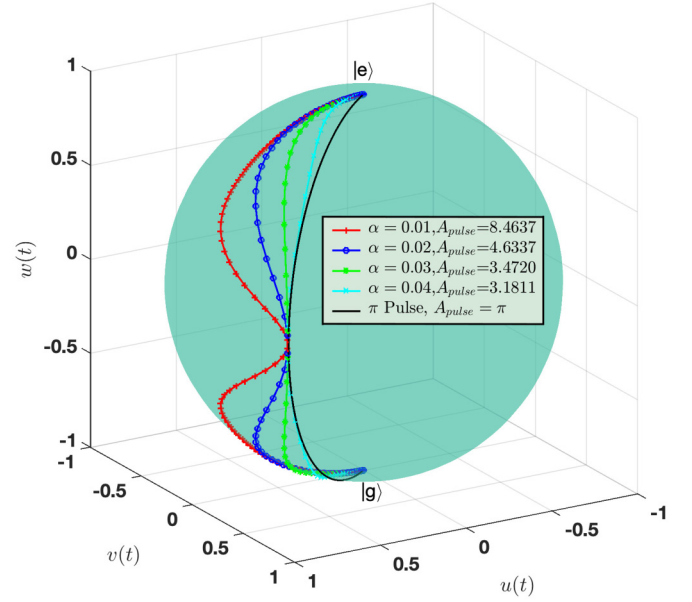


FIG. 2. Different evolution trajectories on the Bloch sphere. The parameters for the trajectories of different  $\alpha$  are  $a_i = 1$ ,  $a_f = -1$ ,  $A = 0.6$  a.u.,  $\tau = 0$  a.u.,  $\sigma = 50$  a.u., and  $\mu = 6$  a.u. The parameters for the trajectory of  $\pi$  pulse are  $\Omega = 1$ ,  $\theta \approx 4.1$ , and  $t = 1$ .

illustrative example is depicted in Fig. 3, in which the parameters are  $a_i = 1$ ,  $a_f = -0.92$ ,  $\alpha = 0.05$  a.u.,  $\omega = 0.5$  a.u.,  $A = 0.5$  a.u.,  $\tau = 0$  a.u.,  $\sigma = 50$  a.u., and  $\mu = 6$  a.u. As shown clearly in Fig. 3(a), the PCF  $w(t)$  (the red-solid line) and the evolution of  $\langle \hat{\sigma}_z \rangle$  (the blue-dash line) are coincident with each other very well. Figure 3(b) shows a comparison of the desired evolution of coherence  $C_A(t)$  and the exact evolution  $C_N(t)$ . As expected, a nearly perfect agreement is observed, with the  $C_A(t)$  (the red-solid line) and  $C_N(t)$  (the blue-dash line) barely discernible. In a word, the evolution of system closely follows the desired one with the designed pulse, which

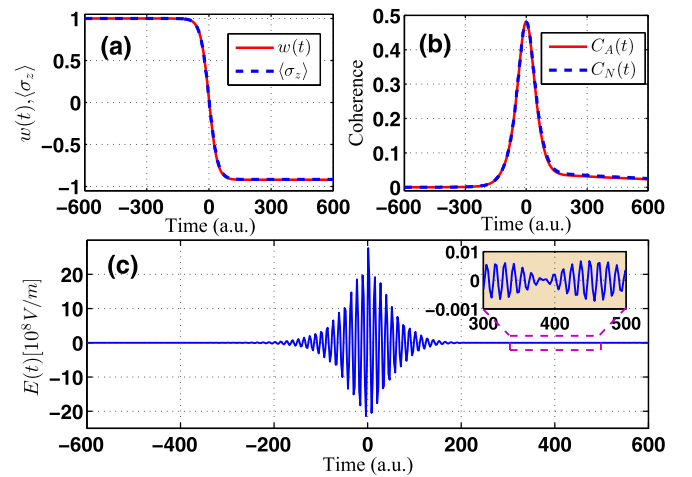


FIG. 3. (a) The PCF  $w(t)$  and  $\langle \hat{\sigma}_z \rangle$ , (b)  $C_A(t)$  and  $C_N(t)$ , as a function of time. (c) The field  $E(t)$  obtained from Eq. (9). The parameters are  $\alpha = 0.05$  a.u.,  $\omega = 0.5$  a.u.,  $A = 0.5$  a.u.,  $\tau = 0$  a.u.,  $\sigma = 50$  a.u.,  $\mu = 6$  a.u.,  $a_i = 1$ ,  $a_f = -0.92$ ,  $\gamma = 0.001$  a.u., and  $\Gamma = \bar{n} = 0$  a.u.



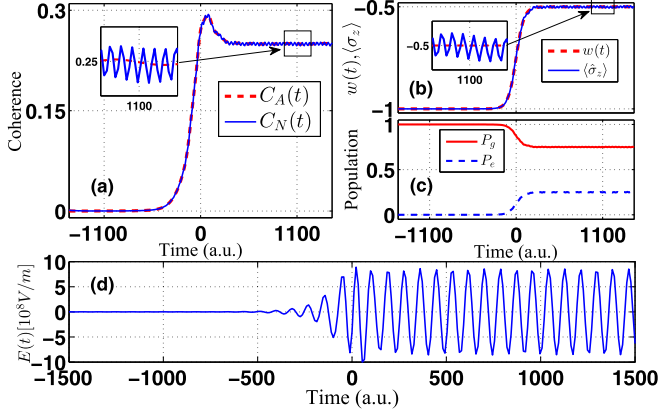


FIG. 4. (a) The  $C_A(t)$  and  $C_N(t)$ , (b) the PCF  $w(t)$  and  $\langle \hat{\sigma}_z \rangle$ , (c) the populations  $P_e$  and  $P_g$ , as a function of time. (d) The field  $E(t)$  obtained from Eq. (9). The parameters are  $\alpha = 0.02$  a.u.,  $\omega = 0.5$  a.u.,  $A = 0.35$  a.u.,  $\tau = 0$  a.u.,  $\sigma = 50$  a.u.,  $a_i = -1$ ,  $a_f = -0.5$ ,  $\bar{n} = 0.0$  a.u., and  $\Gamma = \gamma = 0.005$  a.u.

is shown in Fig. 3(c). The simulation results indicate the good performance of the reverse-engineering scheme in the presence of certain pure dephasing.

Next, we consider the general case wherein both dephasing and thermal noises are involved. One illustrative example is depicted in Fig. 4. The parameters in the simulation are chosen as  $\gamma = \Gamma = 0.005$  a.u.,  $\bar{n} = 0$  a.u.,  $\alpha = 0.02$  a.u.,  $A = 0.35$  a.u.,  $\tau = 0$  a.u.,  $\sigma = 50$  a.u.,  $a_i = -1$ ,  $a_f = -0.5$ . With these parameters, the predefined CCF  $C_A(t)$  and PCF  $w(t)$  are shown by the red-dash line in Figs. 4(a) and 4(b), respectively. It is shown that the  $C_A(t \rightarrow \infty) \simeq 0.25$  and  $w(t \rightarrow \infty) = -0.5$ , which means that the final coherence maintains around 0.25 and final population  $P_e = 1 - P_g = \frac{1-w(t \rightarrow \infty)}{2} = 0.25$ . For comparison, the numerical results of  $C_N(t)$  and  $\langle \sigma_z \rangle$  are also presented by the blue-solid line in Figs. 4(a) and 4(b), respectively. We can note that the evolution of  $C_N(t)$  and  $C_A(t)$  [Fig. 4(a)] as well as  $\langle \sigma_z \rangle$  and  $w(t)$  [Fig. 4(b)] are coincident with each other very well, with only small oscillations in  $C_N(t)$  and  $\langle \sigma_z \rangle$  for long-time evolution. As a result, the system closely follows the desired evolution given by the predefined functions. In Fig. 4(c), we plot the population evolution of  $P_g$  and  $P_e$ . Clearly, the desired final population  $P_e = 0.25$  is obtained. Further observations from Figs. 4(a) and 4(c) suggest that the reverse-engineering scheme is feasible to keep the coherence without losing populations even in the presence of dephasing and thermal noises. Figure 4(d) shows that after achieving the desired population and coherence the pulse strives to maintain the same system state in the presence of dissipation, where the amplitude of pulse is dominated by  $s(t \rightarrow \infty)$ ,  $\dot{s}(t \rightarrow \infty)$  ( $s = u, v, w$ ), and the total decoherence rate  $\tilde{\Gamma}$  according to Eq. (9). Specifically, the amplitude of pulse increases with the increasing of decoherence rate.

#### IV. DISCUSSION

As mentioned above, it is important to know the regime in which the reverse-engineering scheme performs well, i.e., the RWA is well satisfied. To study this issue, by taking the closed system as the example first, in Fig. 5(a) we plot

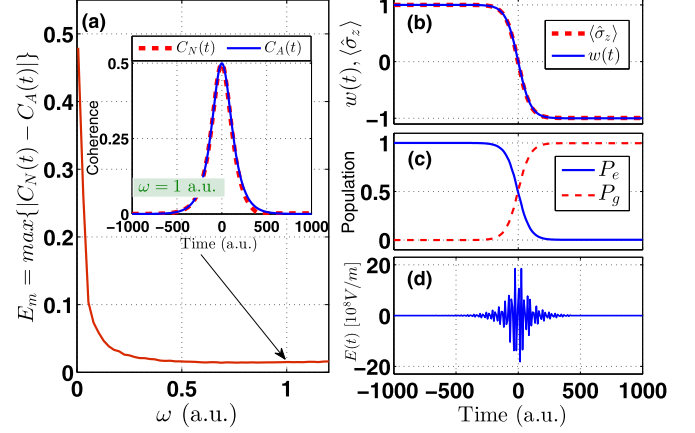


FIG. 5. (a) The maximum error  $E_m$  as a function of  $\omega$ . The inset of (a) shows the analytical and numerical coherence as a function of time in the case of  $\omega = 1$  a.u.. (b) The PCF  $w(t)$  and the  $\langle \hat{\sigma}_z \rangle$  as a function of time. (c) The evolution of  $P_g$  and  $P_e$ . (d) The pulse obtained from Eq. (9) by using the same parameters as in Fig. 1 except  $\omega = 1$  a.u.

the maximum deviation between  $C_N(t)$  and  $C_A(t)$  (defined as  $E_m = \max\{|C_N(t) - C_A(t)|\}$ ) as a function of  $\omega$ . We can see that  $E_m$  approaches the minimum value when  $\omega > 0.5$  a.u., indicating that precisely controlling the evolution of system is obtained. This point is exactly verified by the coherence shown in the inset of Fig. 5(a) and the evolution of  $\langle \hat{\sigma}_z \rangle$  shown in Fig. 5(b) with the RWA being satisfied very well. More concretely, the system closely follows the desired evolution given by the functions  $u(t)$ ,  $v(t)$ , and  $w(t)$ , resulting in  $C_N(t)$  and  $C_A(t)$ ,  $\langle \hat{\sigma}_z \rangle$  and  $w(t)$  coincide with each other perfectly. Figures 5(c) and 5(d) are the evolution of populations and the pulse  $E(t)$ , respectively. Comparing to the populations depicted in Fig. 1(c), the populations here vary smooth when the RWA is satisfied, at the expense of much oscillations for the pulse [see from Figs. 1(d) and 5(d)]. In addition, one may want to know to which extent of the techniques developed in this context can also be implemented in the of open quantum system case. In Fig. 6, we show the maximum error  $E_m$  and  $C_m$  (the maximum deviation between  $w(t)$  and  $\langle \hat{\sigma}_z \rangle$  defined as  $C_m = \max\{|w(t) - \langle \hat{\sigma}_z \rangle|\}$ ) as a function of  $\omega$ . We can see from the Fig. 6 that both  $E_m$  and  $C_m$  decrease with the increase of  $\omega$ , and approach the minimum value when  $\omega > 0.4$ , indicating the reverse-engineering scheme performs well.

In practice, there inevitably exist variations on the system parameters during the driving process. It is thus worthwhile to discuss the robustness of the scheme against such variations. First, we take into consideration the experimental imperfection operations which may induce variations on the pulse, denoting it by  $\delta E(t)$ . To show the influence of  $\delta E(t)$  on the system dynamics, in the case of closed quantum system, we plot the population  $P_g$  and the coherence  $C_N$  versus time and  $\delta E(t)/E(t)$  in Figs. 7(a) and 7(b), respectively. According to the plots, we obtain the following results. (i) The population  $P_g$  is insensitive to the variation  $\delta E(t)$  since  $P_g$  is almost unchange with  $\delta E(t)/E(t)$  varying in the range  $[-0.1, 0.1]$ . This result is in coincidence with the declaration of Ref. [55] that the strength of field only slightly influences the speed of

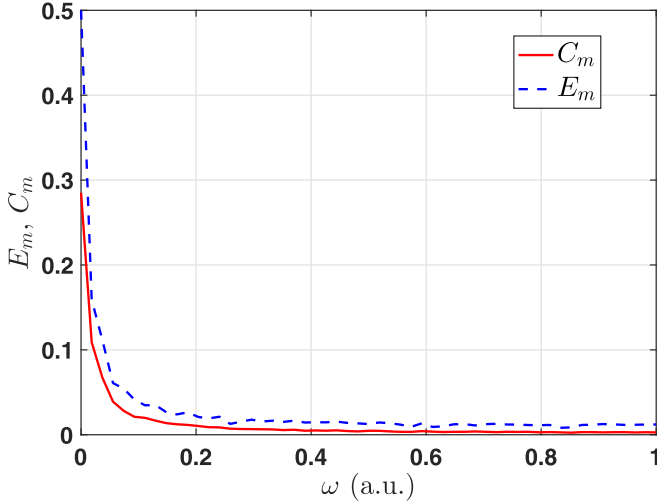


FIG. 6. The maximum error  $E_m$  and  $C_m$  as a function of  $\omega$  in the case of open quantum system. The parameters for the simulation are the same with Fig. 4.

population transition, and it thus would not affect the final population distribution  $P_g(t_f = 1000)$ . (ii) The variation  $\delta E(t)$  has much influence on the coherence due to  $C_N(t_f = 1000) \simeq 0.01$  in the absence of variation while  $C_N(t_f = 1000) \simeq 0.1$  when 10% variation on  $E(t)$  occurring. Next we study the influence of variation on  $\omega$ , denoting by  $\delta\omega$ . The evolutions of population  $P_g$  and coherence  $C_N$  versus time and  $\delta\omega/\omega$  are plotted in Figs. 7(c) and 7(d), respectively. We can see from Figs. 7(c) and 7(d) that both  $P_g$  and  $C_N$  are sensitive to  $\delta\omega/\omega$  since there occurs the amount of deviation of 17% and 25% for the final  $P_g$  and  $C_N$  when  $\delta\omega/\omega = 1\%$ , respectively. Thus, it is necessary to precisely obtain the system parameter  $\omega$  to achieve the desired evolution path.

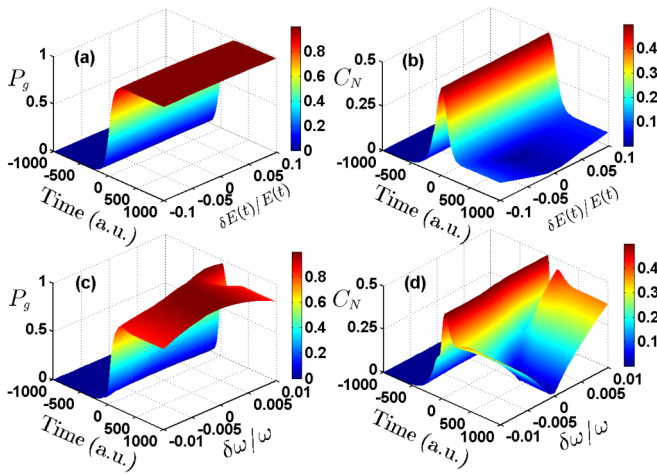


FIG. 7. (a) The population  $P_g$  and (b) the coherence  $C_N$  versus the evolution time and variation of field  $\delta E(t)/E(t)$ . (c) The population  $P_g$  and (d) the coherence  $C_N$  versus the evolution time and  $\delta\omega/\omega$ . The parameters are  $a_i = 1$ ,  $a_f = -1$ ,  $\alpha = 0.02$  a.u.,  $\omega = 1$  a.u.,  $A = 0.6$  a.u.,  $\tau = 0$  a.u.,  $\sigma = 50$  a.u.,  $\Gamma = \gamma = 0$  a.u.,  $\bar{n} = 0.0$  a.u., and  $\mu = 6$  a.u.

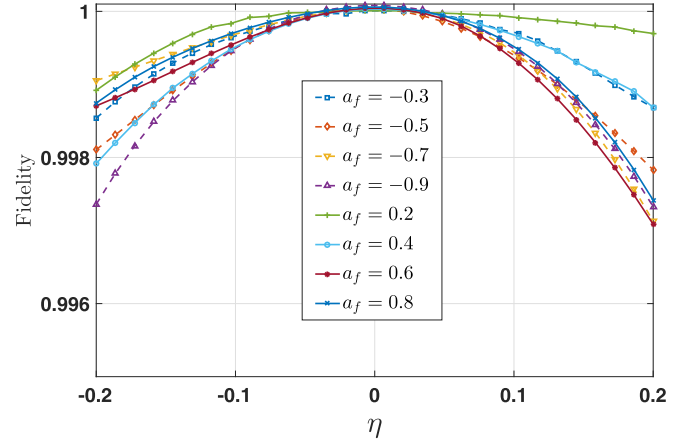


FIG. 8. The fidelity versus  $\eta$  for different final state. The parameters are  $a_i = 1$ ,  $\alpha = 0.02$  a.u.,  $\omega = 1$  a.u.,  $A = 0.6$  a.u.,  $\tau = 0$  a.u.,  $\sigma = 50$  a.u.,  $\Gamma = \gamma = 0$  a.u.,  $\bar{n} = 0.0$  a.u.,  $t_f = 1500$  a.u., and  $\mu = 6$  a.u.

In the above, we showed that the scheme is robust against the variation of pulse intensity when transferring the initial state  $|e\rangle$  to final state  $|g\rangle$ . One may wonder whether this is also true for different final state. In the following, we study how the perturbations on the pulse affect the performance of the scheme for different final state. For the pulse with perturbation, we write it as  $E'(t) = (1 + \eta)E(t)$ , where  $\eta$  quantifies the uncertainty. In Fig. 8, we present the simulation of the fidelity  $F = \sqrt{\langle \hat{\rho}_f | \hat{\rho}(t_f) | \hat{\rho}_f \rangle}$  against the uncertainty  $\eta$  of the pulse for different final state, where  $\hat{\rho}_f$  is the desired final state in the density operator form and  $\hat{\rho}(t_f)$  is the system state in the presence of perturbations at final time  $t_f$ . From Fig. 8, we can observe that the target fidelities are insensitive to the perturbation of the pulse since these fidelities are only slightly changed even when  $\eta = 20\%$ . Therefore, it can be concluded that the robustness against the variation of pulse intensity is quite nice for the population control in the present scheme.

According to Eq. (8c), it is clear that  $u^2 + v^2 + w^2 = c$  ( $c$  is a constant and it is assumed to be unit here) in the case of closed quantum system. Then the function  $u(t) = \pm\sqrt{1 - (v^2 + w^2)}$  is always real with the given functions  $v(t)$  and  $w(t)$  in Sec. III. Thus, it is reasonable to drive an initial state to an arbitrary final state, i.e.,  $a_f$  in the function  $w(t)$  can be arbitrarily chosen in the range of  $[-1, 1]$ . However, in the case of open quantum system, the function  $u(t)$  may exist complex values for some regions of  $a_f$  due to the presence of dissipation, resulting in the complex valued pulse as seen from Eq. (9). The regions of  $a_f$  that lead to complex values of  $u(t)$  are defined as the inaccessible regions since we assumed that the predefined functions  $u(t)$ ,  $v(t)$ ,  $w(t)$  are real. Therefore, the accessible regions of  $a_f$  are to make zero complex values of  $u(t)$ , i.e.,  $\text{Im}[u(t)] = 0$ .

In Fig. 9, we investigate such accessible regions in the presence of dissipation by showing the contour plots of the imaginary part of  $u(t)$  as a function of time and  $a_f$  in Figs. 9(a) to 9(c), and as a function of time and the effective photon number  $\bar{n}$  in Fig. 9(d). Here we fixed  $a_i = -0.6$  corresponding to the initial population of  $P_g = 0.8$  for all of the simulations.

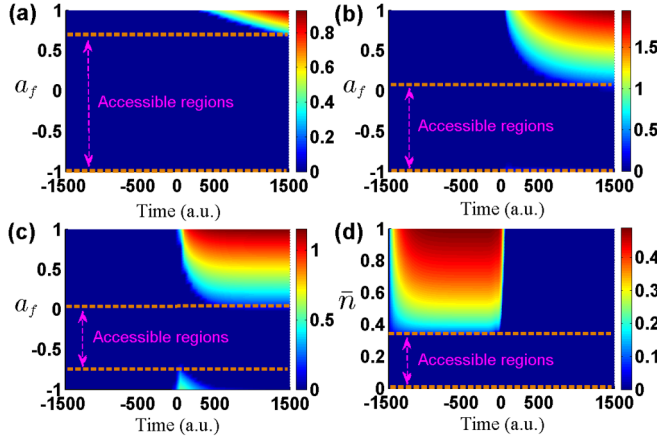


FIG. 9. (a) The imaginary part of  $u(t)$  as function of time and  $a_f$  for  $\Gamma = 0.0001$  a.u.,  $\gamma = 0$  a.u., and  $\bar{n} = 0$  a.u. (b) The imaginary part of  $u(t)$  as a function of time and  $a_f$  for  $\Gamma = 0.001$  a.u.,  $\gamma = 0$  a.u., and  $\bar{n} = 0$  a.u. (c) The imaginary part of  $u(t)$  as a function of time and  $a_f$  for  $\Gamma = 0.001$  a.u.,  $\gamma = 0.001$  a.u., and  $\bar{n} = 0$  a.u. (d) The imaginary part of  $u(t)$  as a function of time and  $\bar{n}$  for  $\Gamma = 0.001$  a.u.,  $\gamma = 0.001$  a.u., and  $a_f = -0.2$ . For all plots, the remaining parameters are the same as Fig. 4 except  $a_i = -0.6$  and  $\alpha = 0.04$  a.u.

In Figs. 9(a) and 9(b), we chose  $\Gamma = 10^{-4}$  a.u. and  $\Gamma = 10^{-3}$  a.u. with  $\gamma = \bar{n} = 0$  a.u., respectively. It is clear that the accessible regions of  $a_f$  are reduced when increasing the thermal noise rate  $\Gamma$ . When further taking the dephasing into consideration, the accessible regions of  $a_f$  are further shrinking, which can be seen by comparing Figs. 9(a) and 9(c). An animation is given in Supplemental Movie, which shows the shrinking process when continuously increase the value of  $\gamma$  [61]. From the animation, one can note that the accessible regions shrink to zero when  $\gamma > 0.01$  a.u. In Fig. 9(d), we consider the influence of the effective photon number  $\bar{n}$  (or equivalently the temperature) on the population transition. Here we fixed  $\Gamma = \gamma = 10^{-4}$  a.u.,  $a_i = -0.6$ , and  $a_f = -0.2$  (corresponds to transferring population of  $P_g = 0.8$  to 0.6). We can see that there is an upper bound  $\bar{n} \simeq 0.33$  for the accessible regions. Of note, the upper bound is different when choosing different parameters of  $a_i$ ,  $a_f$ , as well as  $\Gamma$  and  $\gamma$ . In addition, the accessible regions of  $a_f$  in Figs. 9(a) to 9(c) are

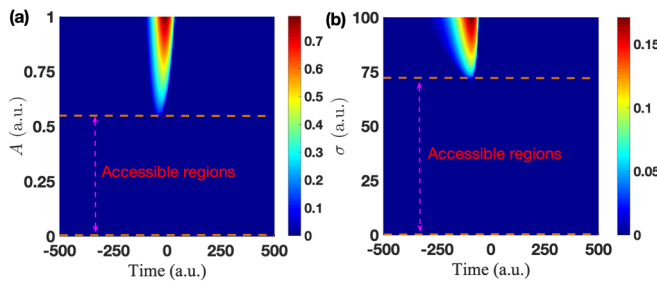


FIG. 10. (a) The imaginary part of  $u(t)$  as a function of time and  $A$  with  $\sigma = 50$  a.u. (b) The imaginary part of  $u(t)$  as a function of time and  $\sigma$   $A = 0.35$  a.u. For all plots, the remaining parameters are  $a_i = -1$ ,  $a_f = -0.5$ ,  $\bar{n} = 0$  a.u.,  $\Gamma = 0.001$  a.u.,  $\gamma = 0.001$  a.u.,  $\mu = 6$  a.u., and  $\alpha = 0.04$  a.u.

TABLE I. Different values of  $a_i$  corresponding to the accessible maximum value of  $a_f$  ( $a_f^M$ ), minimum value of  $a_f$  ( $a_f^m$ ), and the accessible region  $\Delta a_f$ , which is defined as  $\Delta a_f = a_f^M - a_f^m$ . The parameters are  $A = 0.35$  a.u.,  $\tau = 0$  a.u.,  $\sigma = 50$  a.u.,  $\alpha = 0.04$  a.u.,  $\bar{n} = \gamma = 0$  a.u., and  $\Gamma = 0.0001$  a.u.

$a_i$	-0.9	-0.6	-0.3	0	0.3	0.6	0.9
$a_f^M$	0.7551	0.6327	0.5510	0.4694	0.4286	0.3878	0
$a_f^m$	-1	-1	-0.9592	-0.8776	-0.8367	-0.8367	0
$\Delta a_f$	1.7551	1.6327	1.5102	1.3470	1.2653	1.2245	0

also different when starting from different initial states (i.e., the different value of  $a_i$ ) in the presence of dissipation.

One may also wonder how changes in the parameters of  $A$  and  $\sigma$  affect the accessible population regions for a given environmental  $\gamma$  and  $\Gamma$ . To tackle this issue, we display the contour plots of the imaginary part of  $u(t)$  as a function of time and parameter  $A$  in Fig. 10(a) and  $\sigma$  in Fig. 10(b). It can be clearly seen from Fig. 10 that there are large ranges of  $A$  and  $\sigma$  which allow for reaching the desired final populations. However, one should notice that for different evolution trajectories the accessible regions of  $A$  and  $\sigma$  would be different. Thus, even for a fixed  $A$  and  $\sigma$ , the allowed accessible population region will be different on the contrary. In Table I, we list some different  $a_i$  with the corresponding accessible region of  $a_f$ , in which  $a_f^M$  denotes the maximum accessible value of  $a_f$ ,  $a_f^m$  represents the minimum accessible value of  $a_f$ , and  $\Delta a_f = a_f^M - a_f^m$ . It is clear that the accessible region  $\Delta a_f$  decreases with the increasing of  $a_i$ . The reason may originate from the fact that the population of  $P_e$  increases with the increasing of  $a_i$ , which results in more dissipation effect during the system dynamics.

## V. CONCLUSION

In summary, based on the idea of reverse engineering, we proposed a simple scheme to find analytical expressions of the laser pulse for controlling the evolution of two-level systems as desired. The laser pulse is reversely solved based on the general formalism of the density matrix. Thus the scheme sidesteps the consideration of phases of states' amplitude and coherence over previous reverse-engineering methods. The flexibility in choosing the PCF and CCF ensures us to predetermine the evolution of system, and design pulse to control the system as desired. To illustrate the effectiveness of the scheme, we showed several examples in both closed and open quantum systems. Numerical simulation shows that the scheme works well, i.e., the populations and coherence of the system closely follows the desired one, when the RWA is strictly satisfied. Notably, the scheme can be applied to maintain system coherence and populations at the realistic scenarios including dephasing and thermal noises. Additionally, although the focus is on the laser-driven system control, the scheme presented here is general and may be applied for achieving ultrashort laser pulse in the molecule MePeNNA [62] and modulating the magnetic field for population transition in spin systems [63,64], and so on. Finally, we leave open the possibility to generalize the pulse reverse engineering to the case without the rotating-wave approximation [65,66].

## ACKNOWLEDGMENTS

The authors wish to acknowledge helpful discussions with C. S. Hu, B. H. Huang, and Y. H. Kang. This work was

supported by the National Natural Science Foundation of China under Grants No. 11805036, No. 11575045, and No. 11674060, and the Natural Science Foundation of Fujian Province of China under Grant No. 2018J01413.

- 
- [1] S. B. Zheng and G. C. Guo, *Phys. Rev. Lett.* **85**, 2392 (2000).  
 [2] K. Khodjasteh, J. Sastrawan, D. Hayes, T. J. Green, M. J. Biercuk, and L. Viola, *Nat. Commun.* **4**, 2045 (2013).  
 [3] C. P. Koch, M. Lemeshko, and D. Sugny, *Rev. Mod. Phys.* **91**, 035005 (2019).  
 [4] Q. Guo, J. Bai, L. Y. Cheng, X. Q. Shao, H. F. Wang, and S. Zhang, *Phys. Rev. A* **83**, 054303 (2011).  
 [5] S. L. Su, X. Q. Shao, H. F. Wang, and S. Zhang, *Phys. Rev. A* **90**, 054302 (2014).  
 [6] F. Y. Zhang, W. B. Yan, and C. P. Yang, *Phys. Rev. A* **98**, 042331 (2018).  
 [7] X. Q. Shao, D. X. Li, Y. Q. Ji, J. H. Wu, and X. X. Yi, *Phys. Rev. A* **96**, 012328 (2017).  
 [8] V. Macri, F. Nori, and A. F. Kockum, *Phys. Rev. A* **98**, 062327 (2018).  
 [9] M. J. Kastoryano, F. Reiter, and A. S. Sørensen, *Phys. Rev. Lett.* **106**, 090502 (2011).  
 [10] C. Leroux, L. C. G. Govia, and A. A. Clerk, *Phys. Rev. Lett.* **120**, 093602 (2018).  
 [11] K. Bergmann, H. Theuer, and B. W. Shore, *Rev. Mod. Phys.* **70**, 1003 (1998).  
 [12] K. M. Tibbetts and H. Rabitz, *Phys. Chem. Chem. Phys.* **17**, 3164 (2015).  
 [13] J. R. Kuklinski, U. Gaubatz, F. T. Hioe, and K. Bergmann, *Phys. Rev. A* **40**, 6741 (1989).  
 [14] M. Demirplak and S. A. Rice, *J. Phys. Chem. A* **107**, 9937 (2003).  
 [15] X. D. Tian, Y. M. Liu, C. L. Cui, and J. H. Wu, *Phys. Rev. A* **92**, 063411 (2015).  
 [16] M. V. Berry, *J. Phys. A: Math. Theor.* **42**, 365303 (2009); X. Chen, E. Torrontegui, and J. G. Muga, *Phys. Rev. A* **83**, 062116 (2011).  
 [17] M. Lu, Y. Xia, L. T. Shen, J. Song, and N. B. An, *Phys. Rev. A* **89**, 012326 (2014).  
 [18] S. Martínez-Garaot, E. Torrontegui, X. Chen, and J. G. Muga, *Phys. Rev. A* **89**, 053408 (2014).  
 [19] U. Boscain, G. Charlot, J. P. Gauthier, S. Guérin, and H. R. Jauslin, *J. Math. Phys.* **43**, 2107 (2002).  
 [20] N. Khanejaa, T. Reissb, C. Kehlth, T. S. Herbrüggen, and S. J. Glaser, *J. Magn. Reson.* **172**, 296 (2005).  
 [21] S. H. Wu, M. Amezcuca, and H. Wang, *Phys. Rev. A* **99**, 063812 (2019).  
 [22] S. C. Hou, M. A. Khan, X. X. Yi, D. Y. Dong, and I. R. Petersen, *Phys. Rev. A* **86**, 022321 (2012).  
 [23] S. Kuang and S. Cong, *Acta Automat. Sinica* **36**, 1257 (2010); S. Kuang, D. Dong, and I. R. Petersen, *Automatica* **81**, 164 (2017).  
 [24] D. Ran, Z. C. Shi, J. Song, and Y. Xia, *Phys. Rev. A* **96**, 033803 (2017).  
 [25] S. Kuang and S. Cong, *Automatica* **44**, 98 (2008).  
 [26] M. Mirrahimi, P. Rouchon, and G. Turinici, *Automatica* **41**, 1987 (2005).  
 [27] J. M. Coron, A. Grigoriu, C. Lefter, and G. Turinici, *New J. Phys.* **11**, 105034 (2009).  
 [28] Z. C. Shi, X. L. Zhao, and X. X. Yi, *Phys. Rev. A* **91**, 032301 (2015).  
 [29] W. X. Cui, S. Hu, H. F. Wang, A. D. Zhu, and S. Zhang, *Opt. Express* **24**, 15319 (2016).  
 [30] T. Konrad and H. Uys, *Phys. Rev. A* **85**, 012102 (2012); H. Uys, H. Bassa, P. du Toit, S. Ghosh, and T. Konrad, *ibid.* **97**, 060102(R) (2018).  
 [31] D. Vitali, P. Tombesi, and G. J. Milburn, *Phys. Rev. A* **57**, 4930 (1998).  
 [32] N. V. Vitanov, T. Halfmann, B. W. Shore, and K. Bergmann, *Annu. Rev. Phys. Chem.* **52**, 763 (2001).  
 [33] X. Lacour, S. Guerin, L. P. Yatsenko, N. V. Vitanov, and H. R. Jauslin, *Phys. Rev. A* **75**, 033417 (2007).  
 [34] X. J. Lu, X. Chen, A. Ruschhaupt, D. Alonso, S. Guérin, and J. G. Muga, *Phys. Rev. A* **88**, 033406 (2013).  
 [35] S. Ashhab, *Phys. Rev. A* **90**, 062120 (2014).  
 [36] F. Impens and D. Guéry-Odelin, *Sci. Rep.* **9**, 4048 (2019).  
 [37] B. Militello, *Phys. Rev. A* **99**, 063412 (2019).  
 [38] A. Ruschhaupt, X. Chen, D. Alonso, and J. G. Muga, *New J. Phys.* **14**, 093040 (2012).  
 [39] Z. B. Feng, X. J. Lu, M. Li, R. Y. Yan, and Y. Q. Zhou, *New J. Phys.* **19**, 123023 (2017).  
 [40] X. X. Yi, X. L. Huang, C. Wu, and C. H. Oh, *Phys. Rev. A* **80**, 052316 (2009).  
 [41] W. Cui and F. Nori, *Phys. Rev. A* **88**, 063823 (2013).  
 [42] W. Li, C. Li, and H. Song, *Phys. Rev. E* **93**, 062221 (2016).  
 [43] S. Damodarapur, M. Lucamarini, G. Di Giuseppe, D. Vitali, and P. Tombesi, *Phys. Rev. Lett.* **103**, 040502 (2009).  
 [44] M. Lucamarini, G. Di Giuseppe, S. Damodarapur, D. Vitali, and P. Tombesi, *Phys. Rev. A* **83**, 032320 (2011).  
 [45] J. Fischer, D. Basilewitsch, C. P. Koch, and D. Sugny, *Phys. Rev. A* **99**, 033410 (2019).  
 [46] B. Kaufman, T. Paltoo, T. Grogan, T. Pena, J. P. S. John, and M. J. Wright, *Appl. Phys. B* **123**, 58 (2017).  
 [47] H. Jo, H. G. Lee, S. Guérin, and J. Ahn, *Phys. Rev. A* **96**, 033403 (2017).  
 [48] Y. H. Chen, Y. Xia, Q. C. Wu, B. H. Huang, and J. Song, *Phys. Rev. A* **93**, 052109 (2016).  
 [49] N. V. Golubev, V. Despré, and A. I. Kuleff, *J. Mod. Optic.* **64**, 1031 (2017).  
 [50] A. Baksic, H. Ribeiro, and A. A. Clerk, *Phys. Rev. Lett.* **116**, 230503 (2016).  
 [51] X. Chen, I. Lizuain, A. Ruschhaupt, D. Guéry-Odelin, and J. G. Muga, *Phys. Rev. Lett.* **105**, 123003 (2010); X. Chen and J. G. Muga, *Phys. Rev. A* **86**, 033405 (2012).  
 [52] H. L. Mortensen, J. J. W. Sørensen, K. Mølmer, and J. F. Sherson, *New J. Phys.* **20**, 025009 (2018).  
 [53] F. Petiziol, B. Dive, F. Mintert, and S. Wimberger, *Phys. Rev. A* **98**, 043436 (2018).



- [54] D. Daems, A. Ruschhaupt, D. Sugny, and S. Guerin, *Phys. Rev. Lett.* **111**, 050404 (2013).
- [55] N. V. Golubev and A. I. Kuleff, *Phys. Rev. A* **90**, 035401 (2014).
- [56] N. V. Golubev and A. I. Kuleff, *Phys. Rev. A* **91**, 051401(R) (2015).
- [57] I. Medina and F. L. Semião, *Phys. Rev. A* **100**, 012103 (2019).
- [58] S. M. Barnett and P. M. Radmore, *Methods in Theoretical Quantum Optics* (Clarendon, New York, 1997).
- [59] H. J. Carmichael, *Statistical Methods in Quantum Optics: Master Equations and Fokker-Planck Equations* (Springer-Verlag, Berlin, 1999).
- [60] K. N. Zlatanov, G. S. Vasilev, P. A. Ivanov, and N. V. Vitanov, *Phys. Rev. A* **92**, 043404 (2015).
- [61] See Supplemental Material at <http://link.aps.org/supplemental/10.1103/PhysRevA.101.023822> for more information on the shrinking process.
- [62] S. Lünemann, A. I. Kuleff, and L. S. Cederbaum, *J. Chem. Phys.* **129**, 104305 (2008); A. I. Kuleff and L. S. Cederbaum, *Phys. Rev. Lett.* **106**, 053001 (2011).
- [63] F. Y. Zhang and C. P. Yang, *Opt. Lett.* **43**, 466 (2018).
- [64] Q. Zhang, X. Chen, and D. Guéry-Odelin, *Sci. Rep.* **7**, 15814 (2017).
- [65] S. Ibáñez, Y. C. Li, X. Chen, and J. G. Muga, *Phys. Rev. A* **92**, 062136 (2015).
- [66] Q. C. Wu, Y. H. Chen, B. H. Huang, Z. C. Shi, J. Song, and Y. Xia, *Ann. Phys. (NY)* **529**, 1700186 (2017).